ACS APPLIED MATERIALS & INTERFACES

Research Article

Cite This: ACS Appl. Mater. Interfaces 2018, 10, 6560−6569

www.acsami.org

FRET Effect between Fluorescent Polydopamine Nanoparticles and MnO_2 Nanosheets and Its Application for Sensitive Sensing of Alkaline Phosphatase

Ting Xiao,[†,‡] Jian Sun,[†] Jiahui Zhao,[†,§] Shuang Wang,[†,‡] Guoyong Liu,[†,‡] and Xiurong Yang*[,†]

[†]State Key Laboratory of Electroanalytical Chemistry, Changchun Institute of Applied Chemistry, Chinese Academy of Sciences, Changchun, Jilin 130022, China

[‡]University of Science and Technology of China, Hefei, Anhui 230026, China

[§]University of Chinese Academy of Sciences, Beijing 100049, China

Supporting Information

ABSTRACT: As an essential and universal hydrolase, alkaline phosphatase (ALP) has been identified as a crucial indicator of various diseases. Herein, we, for the first time, expanded the application of fluorescent polydopamine (F-PDA) nanoparticles to nanoquencher-based biosensing system, as well as discovered the reversible quenching effect of manganese dioxide (MnO_2) nanosheets on the fluorescence of F-PDA nanoparticles and intensively confirmed the quenching mechanism of Förster resonance energy transfer by using transmission electron microscopy, UV−vis, Fourier transform infrared spectroscopy, and fluorescence lifetime experiments. By means of the ALP-triggered generation of ascorbic acid (AA) from the substrate ascorbic acid 2-phosphate, the AA-triggered reduction of MnO_2 nanosheets to Mn^{2+}, as well as the clear quenching mechanism of F-PDA nanoparticles by MnO_2 nanosheets, we have developed a label-free, low-cost, visual, and facile synthetic fluorescent biosensor for convenient assay of ALP activity. The fluorescent bioassay shows a good linear relationship from 1 to 80 mU/mL (R^2 = 0.999), with a low detection limit of 0.34 mU/mL, and the excellent applicability in human serum samples demonstrates potential applications in clinical diagnosis and biomedical research.

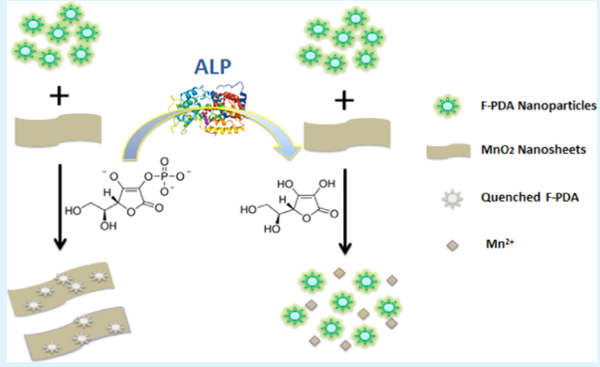

KEYWORDS: *fluorescent polydopamine nanoparticle, MnO_2 nanosheets, Förster resonance energy transfer, alkaline phosphatase, fluorescent probe*

INTRODUCTION

Alkaline phosphatase (ALP) is an essential and universal hydrolase that is responsible for the cleavage of the phosphate functional groups from a wide variety of substrate molecules.[1] This process plays crucial roles in intracellular signal transmission and protein activity regulation.[2−4] This enzyme has been confirmed as a crucial serum biochemical indicator in the diagnosis of various diseases, such as diabetes mellitus,[5] liver disease,[6] Alzheimer's disease,[7] bone metastasis from prostate carcinoma,[8] and so on. Therefore, developing convenient and sensitive sensing of ALP will benefit the diagnoses of diseases and biomedical research. To date, a large number of analytical methods have been established for ALP detection, including colorimetric,[9,10] fluorescence,[11,12] electrochemistry,[13,14] electrochemiluminescence,[15] surface enhancement Raman scattering,[16,17] and chromatography.[18] Among them, fluorescent probes are extremely attractive and promising because of their simplicity, high sensitivity, rapid implementation, and real-time detection. Up to now, various fluorescent probes have been reported for ALP detection by using organic dyes,[19,20] quantum dots (QDs),[21−23] noble metal nanoclusters,[24,25] and coordination polymers[26,27] as fluorescent materials. Although great achievements have been made, the above systems suffer some drawbacks, such as poor water solubility and bad photostability of dyes, high toxicity of QDs, high costs and poor stability of noble metal nanoclusters, and a complex synthesis process and surface modification of coordination polymers. Undoubtedly, it is still challenging to find a suitable fluorescent probe for monitoring ALP levels, especially taking advantage of facile and rapid synthesis of fluorescent materials with nontoxicity, cost-effectiveness, good water solubility, and photostability.

Most notably, fluorescent polymer nanoparticles have emerged as a kind of promising material recently due to their striking stability, nontoxic nature, and well-controlled surface properties.[28,29] Particularly, naturally generated and label-free

Received: December 11, 2017
Accepted: January 31, 2018
Published: January 31, 2018

DOI: 10.1021/acsami.7b18816
ACS Appl. Mater. Interfaces 2018, 10, 6560−6569

Scheme 1. Schematic Illustration of the F-PDA−MnO_2 Probe for ALP Detection on the Basis of FRET

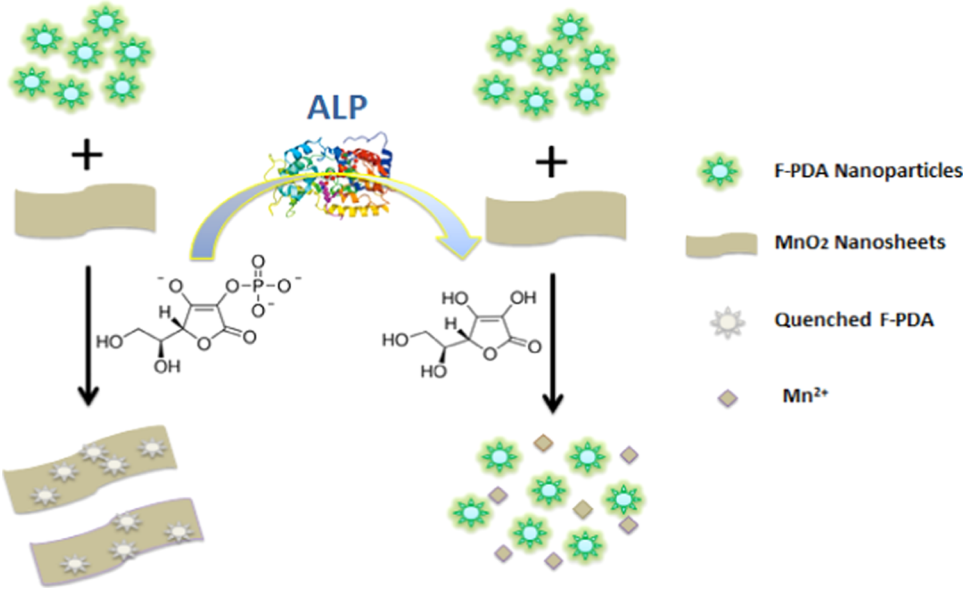

fluorescent polymer without any surface modification is greatly attractive and significant.[30,31] Dopamine is a critical neurotransmitter in the brain, which plays physiological roles in neurotransmission and hormone release control.[32] Under oxidative stress or alkaline (pH > 7.5) conditions, dopamine is susceptible to be polymerized into polydopamine (PDA) nanoparticles through covalent bonding, hydrogen bonding, $\pi-\pi$ interactions, and so on.[31,33] Not only owing to their striking properties of optics, electricity, and magnetics but also due to the excellent biocompatibility and biodegradability, PDA has become a kind of novel biopolymerized material and has been extensively used in diverse fields, such as materials science, energy, water treatment, biomedical science, and others.[34−38] Up to now, only a few reports focused on the application of the intrinsic fluorescent polydopamine (F-PDA) nanoparticles in the biosensing system. To the best of our knowledge, the sensing mechanisms of these studies were mostly about monitoring the intrinsic fluorescence of in situ synthesized F-PDA nanoparticles under the aid of oxidants,[30,39,40] the formation of F-PDA dots from hydroxyl radical-induced degradation of polydopamine nanoparticles,[41] or the redox reaction between Fe^{2+} and F-PDA nanoparticles.[31] However, the application based on the interaction of F-PDA nanoparticles and the nanoquencher materials (such as gold nanoparticles, graphene oxide, carbon nanotubes, transition metal sulfide nanosheets, and so on) has not been reported so far.

Recently, as a kind of inorganic two-dimensional nanomaterial, manganese dioxide (MnO_2) nanosheets have attracted great attention and usually been used as an effective fluorescent nanoquencher for biosensing due to their striking advantages, including low cost, good biocompatibility and chemical stability, high specific capacitance and surface area, and broad absorption spectrum (210−600 nm) with a large molar extinction coefficient (ε_{max} = 9.6 × 10^3 M^{-1} cm^{-1}).[42−44]

Herein, we, for the first time, expanded the application of F-PDA nanoparticles to a nanoquencher-based biosensing system, as well as discovered the reversible quenching effect of MnO_2 nanosheets on the fluorescence of F-PDA nanoparticles and intensively confirmed the quenching mechanism of the Förster resonance energy transfer (FRET) by using transmission electron microscopy (TEM), UV−vis, Fourier transform infrared (FT-IR) spectroscopy and fluorescence lifetime experiments. With F-PDA nanoparticles serving as the fluorescent donor and MnO_2 nanosheets as the fluorescent receptor to form an FRET pair, the fluorescence of F-PDA nanoparticles was efficiently quenched by the MnO_2 nanosheets in the form of exponential decay. Meanwhile, ALP could catalyze the hydrolysis of 2-phospho-L-ascorbic acid (AA2P) to generate L-ascorbic acid (AA), which could reduce MnO_2 into Mn^{2+} and trigger the decomposition of MnO_2 nanosheets, accompanied with the fluorescence recovery of F-PDA nanoparticles. On the basis of the above reaction process, a label-free, low-cost, visual, and specific detection of ALP was strikingly achieved for the first time (Scheme 1). This biosensor exhibits good sensing performance for the ALP assay, with a wide linear range of 1−80 mU/mL (R^2 = 0.999) and a low detection limit of 0.34 mU/mL as well as excellent selectivity. Moreover, the excellent applicability in human serum samples demonstrates potential applications in clinical diagnosis and biomedical research.

EXPERIMENTAL SECTION

Chemicals and Materials. L-Ascorbic acid (AA) was purchased from Dingguo Biotechnology Company (Beijing, China). Alkaline phosphatase (ALP) from bovine intestinal mucosa, dopamine hydrochloride, peroxidase from horseradish (HRP), bovine serum albumin (BSA), human serum albumin (HSA), acetylcholinesterase (AChE), lysozyme, IgG (from human serum), glucose oxidase (GOx), trypsin and reduced *N*-ethylmaleimide (NEM) were purchased from Sigma-Aldrich (St. Louis, MO). L -Ascorbic acid 2-phosphate trisodium salt and tetramethylammonium hydroxide (TMA·OH) were purchased from Aladdin Industrial Corporation (Shanghai, China). $MnCl_2·4H_2O$ and H_2O_2 (30%) were obtained from Beijing Chemical Corporation (Beijing, China). All of the other chemicals were analytical grade and used as received without any further purification. The ultrapure water from a Millipore system was used throughout all of the experiments.

Apparatus and Characterization. Fluorescence measurements were performed on a Hitachi F-4600 spectrofluorometer (Tokyo, Japan). UV−vis absorption characterization was obtained with a CARY 500 UV−vis−NIR Varian spectrophotometer (CA). TEM images were acquired by H-600 (Hitachi, Tokyo, Japan), with an accelerating

DOI: 10.1021/acsami.7b18816
ACS Appl. Mater. Interfaces 2018, 10, 6560−6569

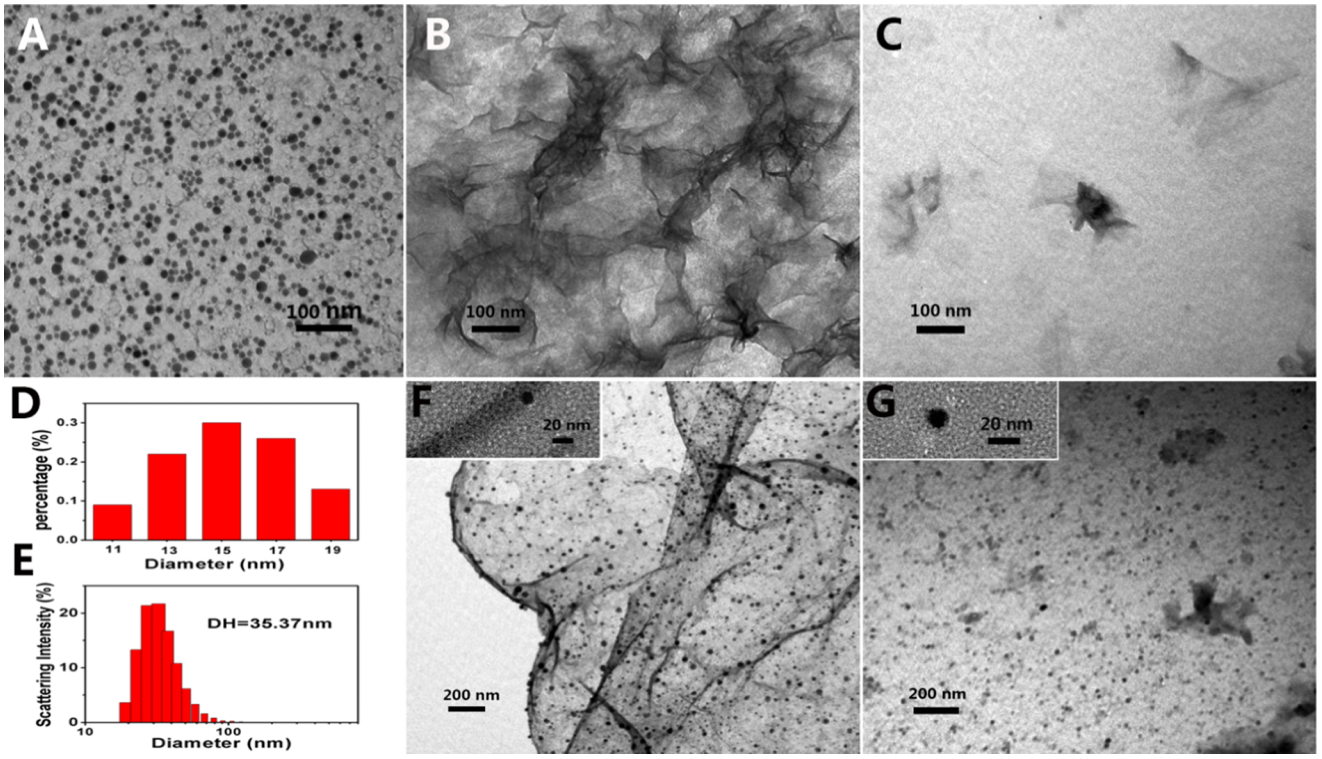

Figure 1. TEM images of (A) F-PDA nanoparticles, (B) MnO_2 nanosheets, and (C) MnO_2 nanosheets in the presence of AA. (D) Size distribution of F-PDA nanoparticles in diameter measured by TEM. (E) Characterization of hydrodynamic size distribution of F-PDA nanoparticles by DLS technique. TEM images of (F) F-PDA–MnO_2 nanocomposites and (G) F-PDA–MnO_2 nanocomposites in the presence of AA (the insets were the HRTEM images of (F) a single F-PDA–MnO_2 nanocomposite and (G) a single released F-PDA nanoparticle under high resolution).

voltage of 100 kV. High-resolution TEM (HRTEM) were taken by a JEM-2010 (HR) microscope operated at 200 kV. FT-IR spectra were obtained using a Bruker Optics VERTEX 70 spectrometer (Ettlingen, Germany) in the transmission mode. The hydrodynamic diameter was performed with a Zetasizer Nano ZS dynamic light scattering (DLS) system (Malvern Instruments Ltd., England). The fluorescence lifetime was obtained on the Horiba-Jobin-Yvon Fluorolog-3 spectrofluorometer (NJ).

Synthesis of F-PDA Nanoparticles. F-PDA nanoparticles were synthesized according to the previously reported methods with a minor modification.[31] Briefly, 400 μL of dopamine hydrochloride aqueous solution (20 mM) and 320 μL of sodium hydroxide solution (100 mM) were added to 7.08 mL of phosphate buffer (PB) (pH 7.4, 2 mM); then, the mixture was transferred into a 20 mL glass vial via magnetic stirring (700 rpm) at room temperature for 1 h to form F-PDA nanoparticles by oxidative polymerization. After this, 200 μL of hydrochloric acid (0.2 M) was added into the solution to sharply slow down the polymerization speed. After an additional 0.5 h, the resulting bright brown solution was stored in dark at room temperature for future use.

Preparation of MnO_2 Nanosheets. The simple synthesis of MnO_2 nanosheets was performed by the previously reported method.[43] Typically, 10 mL of $MnCl_2{\cdot}4H_2O$ (0.3 M) and 20 mL of TMA·OH (0.6 M) containing 3 wt % of H_2O_2 were immediately mixed in a 100 mL round-bottomed flask. The obtained dark brown solution was stirred vigorously in the open air at room temperature for 12 h, and MnO_2 nanosheets were obtained after centrifugation at 10 000 rpm for 15 min, then washed five times with ultrapure water and methanol, respectively. Finally, the precipitate was dried at 50 °C. After dispersing in ultrapure water, the resulting suspension was ultrasonicated to form a brown colloid.

F-PDA Nanoparticles Quenched by MnO_2 Nanosheets. MnO_2 nanosheets solution (351 μg/mL) at various volumes (0, 10, 20, 30, 40, 50, 60, 70, 80, 90, 100, and 110 μL, respectively) were added into 50 μL of F-PDA nanoparticles, and the final volume was adjusted to 500 μL with PB (pH 7.4, 10 mM). Then, the mixture was incubated for 2 min at 37 °C, and the fluorescence emission spectra were measured.

Sensing ALP Activity. For the fluorescent ALP activity assay, 70 μL of MnO_2 nanosheets solution (351 μg/mL) and 50 μL of F-PDA nanoparticles were added to 340 μL of PB (pH 7.4, 10 mM) and incubated for 2 min at 37 °C. Then, 30 μL of AA2P solution (50 mM) and 10 μL of ALP at different concentrations (final concentration 0, 1, 5, 10, 20, 40, 60, 80, 100, 120, and 150 mU/mL, respectively) were mixed with the above F-PDA–MnO_2 nanocomposites. After reacting in the dark for about 40 min at 37 °C, the fluorescence spectra of different samples were recorded from 435 to 550 nm after being excited at 415 nm and the excitation and emission slits were set at 10 nm.

ALP Activity Assay in Human Serum Samples. The human serum was diluted 20 times with PB (pH 7.4, 10 mM). Then, different concentrations of ALP in the linear range were spiked with the above human serum solution containing NEM (0.3 mM) and used for recovery tests.

RESULTS AND DISCUSSION

Characterization of the Synthesized F-PDA Nanoparticles and MnO_2 Nanosheets. The microstructure and morphology of as-synthesized F-PDA nanoparticles were confirmed by the typical TEM image. As shown in Figure 1A, the as-synthesized F-PDA nanoparticles exhibited a good spherical shape and the diameter of the particles measured by TEM was about 11–19 nm, with an average diameter of 15.24 nm (Figure 1D), whereas the hydrodynamic size of F-PDA nanoparticles was 35.37 nm in average performed by DLS (Figure 1E). Particularly, the F-PDA nanoparticles possessed high stability and excellent monodispersity in water solution. In addition, we investigated the surface chemical groups of as-

DOI: 10.1021/acsami.7b18816
ACS Appl. Mater. Interfaces 2018, 10, 6560–6569

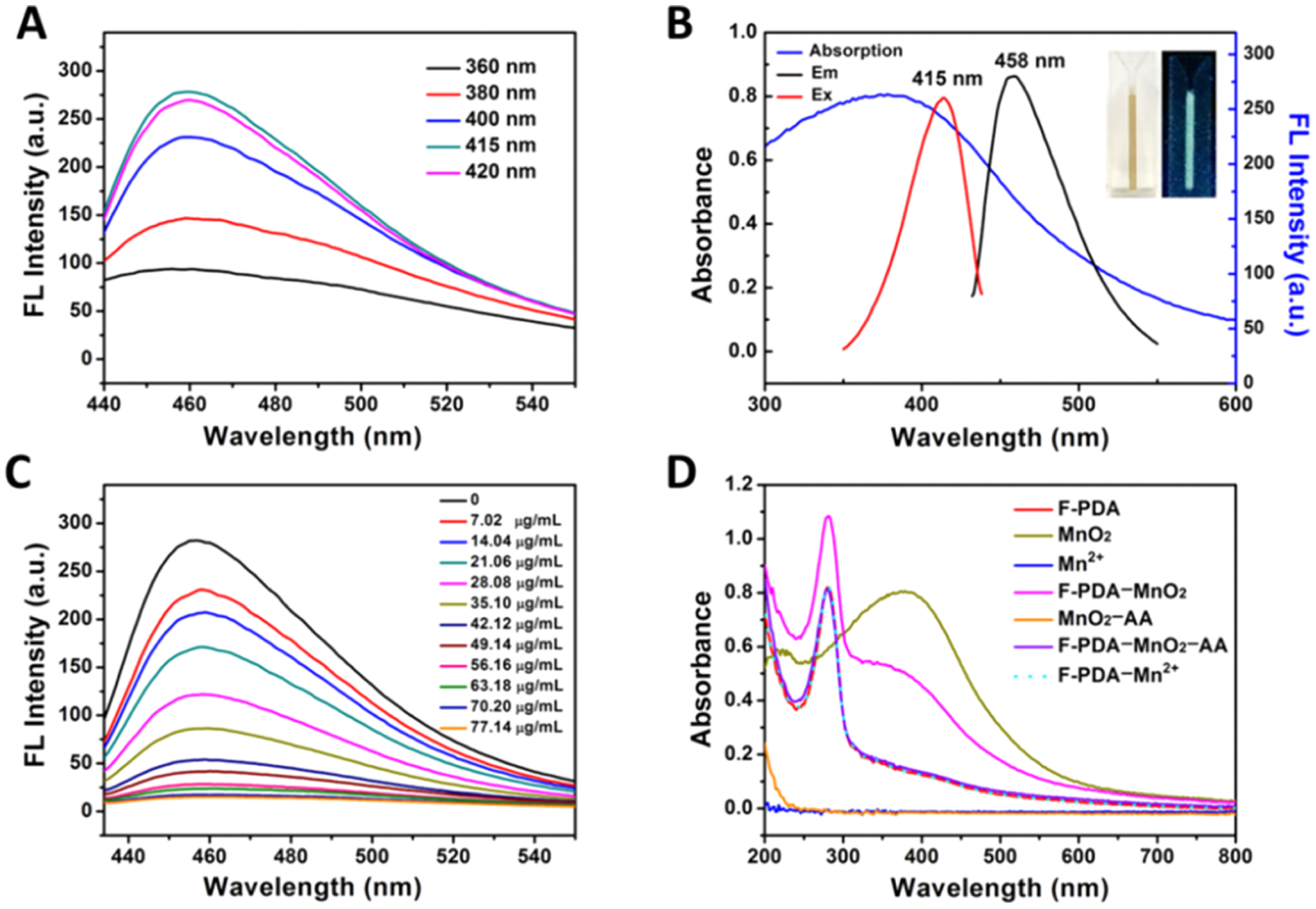

Figure 2. (A) Fluorescence emission spectra of F-PDA nanoparticles under different excitation wavelengths. (B) Excitation and emission spectra of F-PDA nanoparticles and UV−vis absorption spectrum of MnO_2 nanosheets. The inset showed the photographs of F-PDA nanoparticles under room light and UV irradiation. (C) Fluorescence emission spectra of F-PDA nanoparticles in the presence of different concentrations of MnO_2 nanosheets. (D) UV−vis absorption spectra of different substances and systems.

prepared F-PDA nanoparticles via FT-IR spectroscopy (Figure S1). The strong and broad band at 3419 cm^{-1} and the single peak located at 1410 cm^{-1} were ascribed to the characteristic stretching modes of N−H bond, and the peak at 1632 cm^{-1} was attributed to the −C═C− stretching vibrations on indole ring, indicating the specific structure of polyindole. The band located at about 1110 cm^{-1} was assigned to the vibration modes of C−N bond.[31,45] The results also confirmed that the dopamine oxidative polymerization reaction was successfully performed and the large number of hydrophilic groups (−OH, $-NH_2$) on the surface of F-PDA nanoparticles resulted in the excellent water solubility. Furthermore, fluorescence spectra were performed to examine the optical properties of as-prepared F-PDA nanoparticles. Apparently, there was only one emission peak for F-PDA nanoparticles at around 458 nm when excited at different wavelengths ranging from 360 to 420 nm and the maximum excitation was located at 415 nm. Thus, the fluorescence emission of F-PDA nanoparticles was excitation-independent (Figure 2A). The inset in Figure 2B showed the photographs of F-PDA nanoparticles solution under natural light and UV lamp at 365 nm; the bright cyanic under UV irradiation further confirmed the formation of F-PDA nanoparticles. All of the above adequately proved the successful preparation of F-PDA nanoparticles. In addition, fluorescence stability of as-prepared F-PDA nanoparticles was examined. As demonstrated in Figure S2, the fluorescence intensity of F-PDA nanoparticles remained relatively stable after 60 min of irradiation under 365 nm ultraviolet light, indicating their outstanding photostability and potential application for bioanalysis. Moreover, we also investigated the effects of the pH values ranging from 3.0 to 10.0 on the fluorescence intensity of F-PDA nanoparticles. The results showed that the F-PDA nanoparticles exhibited the highest fluorescence intensity at about pH 7.0 and nearly remained stable under alkaline condition but the lower fluorescence intensity was obtained with the lower pH values in acidic condition (Figure S3). Considering the fluorescence intensity and the physiological environment, pH 7.4 was selected as the pH value of the system in the following experiments.

As shown in Figure 1B, the TEM result showed the newly prepared MnO_2 nanosheets presented an obvious two-dimensional sheetlike morphology and the FT-IR absorption peak of as-prepared MnO_2 nanosheets located at 515 cm^{-1} was attributed to the stretching vibration modes of Mn−O bond (Figure S1),[43] fully indicating the formation of MnO_2 nanosheets. In addition, the remarkable optical properties of MnO_2 nanosheets were confirmed by UV−vis absorption. As presented in Figure 2B, the absorbance spectrum displayed a broad band ranging from 300 to 600 nm, with a peak centered at 380 nm, which overlapped well with the fluorescence excitation and emission of F-PDA nanoparticles. The broad absorption could make it feasible as the energy acceptor to F-PDA nanoparticles.

DOI: 10.1021/acsami.7b18816
ACS Appl. Mater. Interfaces 2018, 10, 6560−6569

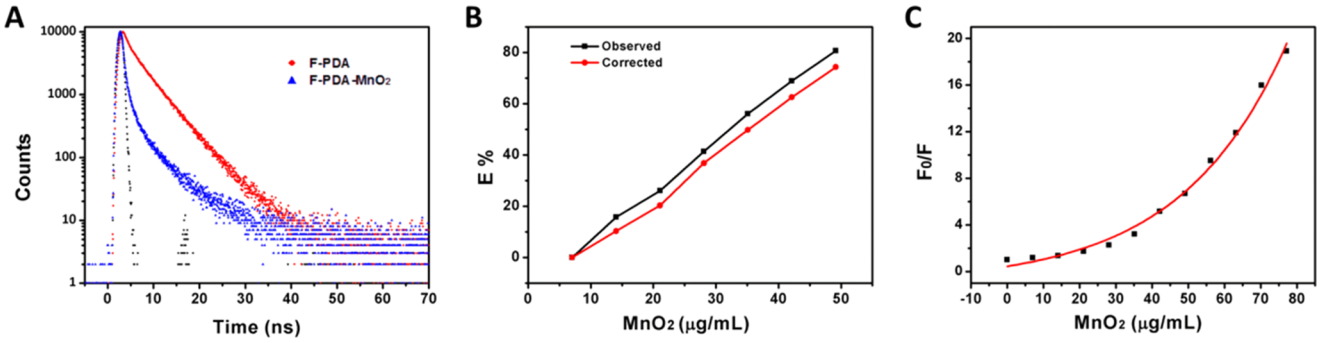

Figure 3. (A) Decay curves of F-PDA nanoparticles in the absence (red curve) and presence (blue curve) of MnO_2 nanosheets. λ_{ex} = 365 nm and λ_{em} = 455 nm (B) the observed quenching efficiency (black curve) and the corrected quenching efficiency by removing the contribution of IFE (red curve) of F-PDA nanoparticles toward different concentrations of MnO_2 nanosheets. (C) Fluorescence change of F-PDA nanoparticles at 458 nm with various concentrations of MnO_2 nanosheets and the red curve was the exponential fitting curve of the plot.

Verification of the Interaction between F-PDA Nanoparticles and MnO_2 Nanosheets. As displayed in Figure 2C, the fluorescence intensity at 458 nm of F-PDA nanoparticles decreased gradually along with the addition of MnO_2 nanosheets because F-PDA nanoparticles were easily adsorbed on the MnO_2 surface to form F-PDA−MnO_2 nanocomposites in solutions. As can be seen in Figure 1F, the F-PDA nanoparticles dispersed homogeneously on the MnO_2 nanosheets. Furthermore, we investigated the UV−vis absorption spectrum of F-PDA−MnO_2 nanocomposites (Figure 2D), which showed two characteristic absorption peaks; one peak located at 280 nm was the characteristic absorption of F-PDA nanoparticles and another centered at 380 nm was the characteristic absorption of MnO_2 nanosheets. Accordingly, the FT-IR spectrum of F-PDA−MnO_2 nanocomposites also contained both the characteristic absorption peaks of F-PDA nanoparticles and MnO_2 nanosheets, such as peaks located at 1632, 1410, and 1110 cm^{-1} of F-PDA and 515 cm^{-1} of MnO_2, and no other obvious new absorption peaks appeared in the F-PDA−MnO_2 nanocomposites (Figure S1). The results above suggested there were no new substances formed in this quenching system.

Quenching Mechanism of F-PDA Nanoparticles by MnO_2 Nanosheets. Generally, FRET, inner filter effect (IFE), dynamic quenching effect (DQE), and static quenching effect (SQE) could cause the fluorescence quenching of fluorescent materials by MnO_2 nanosheets.[44,46] To understand the exact mechanism of F-PDA nanoparticles quenched by MnO_2 nanosheets, the following experiments were carried out.

PDA possesses many functional groups, including planar indole units, *o*-quinone, carboxy, amino, imine, and phenol groups, which may specifically explain the robust adhesion capability of PDA to virtually all types of surfaces, regardless of the substrate's chemistry.[33] On the basis of the inherent adhesive property of PDA, F-PDA nanoparticles were easily adsorbed onto the surface of MnO_2 nanosheets and formed F-PDA−MnO_2 nanocomposites via noncovalent binding interaction (Supporting Information) and HRTEM image of this nanocomposite (Figure 1F) clearly indicated the adhesion of F-PDA on the MnO_2 surface. In addition, as depicted in Figure 2B, there was a relative large overlap region between the broad absorbance spectrum in the range of 300−600 nm of MnO_2 nanosheets and the fluorescence emission spectrum of F-PDA nanoparticles and the overlap integral was 2.61 × 10^{14} M^{-1} cm^{-1} nm^4 by calculation (Supporting Information). Thus, the quenching mechanism of F-PDA nanoparticles by MnO_2 nanosheets was first considered to stem from FRET.[47,48] To further demonstrate this hypothesis, we measured the lifetimes of F-PDA nanoparticles in the absence and presence of MnO_2 nanosheets and the fluorescence lifetime of F-PDA nanoparticles obviously decreased when the MnO_2 nanosheets were added (Figure 3A). Summing up the above, FRET contributed to the fluorescence quenching mechanism of F-PDA nanoparticles by MnO_2 nanosheets.

Owing to the large overlaps between absorbance of MnO_2 nanosheets and excitation of F-PDA nanoparticles (Figure 2B), the role of IFE in the entire quenching process in our system was also investigated. Considering the cuvette geometry used in our fluorescent measurements, the quenching efficiency from IFE was carefully calculated (see detailed analysis in the Supporting Information). The observed quenching efficiency and the corrected quenching efficiency by removing the contribution of IFE were figured out after different concentrations of MnO_2 nanosheets were added into the F-PDA nanoparticle solution. As shown in Figure 3B, we found that there was no significant difference between the observed and the corrected fluorescence quenching efficiency at each concentration of MnO_2 nanosheets. The results strongly indicated that IFE was almost no contribution to the fluorescence quenching process.

Moreover, as reported, the fluorophore forms a nonfluorescent complex with the quencher in a static quenching process. When this complex absorbs light, it immediately returns to the ground state without photon emission,[46] and we discovered that no new absorption peaks appeared in the F-PDA−MnO_2 nanocomposites according to FT-IR spectra (Figure S1) and UV−vis spectra (Figure 2D), which indicated that there were no nonfluorescent fluorophore/quencher complexes formed in this quenching system. Thus, the SQE might not be possibly responsible for the fluorescence quenching either.

In DQE, the excited-state fluorophore is nonradiatively deactivated upon collision with the quencher.[46] DQE could be theoretically described by the Stern−Volmer equation.

$$F_0/F = 1 + K_{SV}[Q]$$

where [Q] is the concentration of quencher, i.e., MnO_2 nanosheets in this system; F_0 and F represent the fluorescence intensity of F-PDA nanoparticles in the absence and presence of MnO_2 nanosheets, respectively. To verify whether the quenching mechanism belongs to DQE or not, we plotted the fluorescence intensity ratio (F_0/F) as a function of concen-

DOI: 10.1021/acsami.7b18816
ACS Appl. Mater. Interfaces 2018, 10, 6560−6569

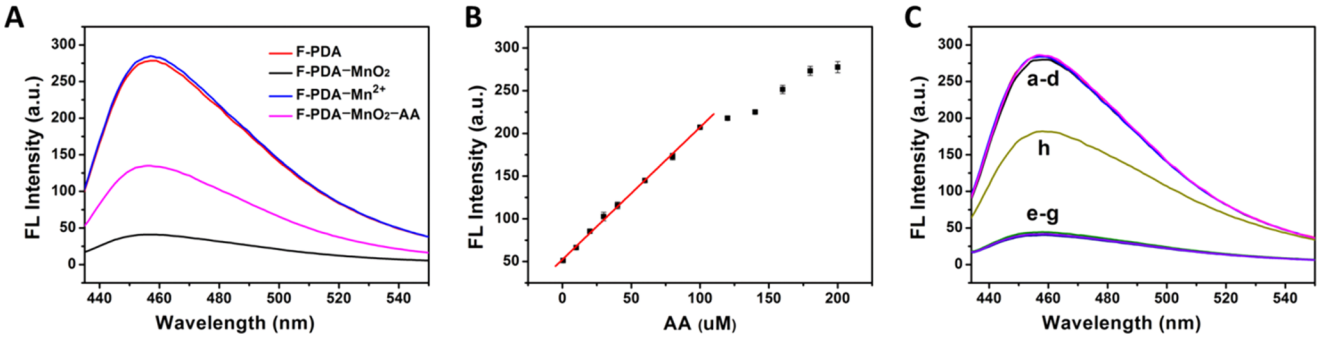

Figure 4. (A) Fluorescence emission spectra of F-PDA nanoparticles under different circumstances. (B) Fluorescence intensities at 458 nm versus different AA concentrations (1, 10, 20, 30, 40, 60, 80, 100, 120, 140, 160, 180, and 200 μM). (C) Fluorescence emission spectra of PDA nanoparticles in the presence of (a) no reactants, (b) AA2P, (c) ALP, (d) AA2P and ALP, (e) MnO_2 nanosheets, (f) MnO_2 nanosheets and AA2P, (g) MnO_2 nanosheets and ALP, and (h) MnO_2 nanosheets, ALP, and AA2P (the concentrations of MnO_2 nanosheets, Mn^{2+}, AA, AA2P, and ALP were 49.14 μg/mL, 0.5 mM, 60 μM, 3 mM, and 60 mU/mL, respectively. The concentrations of F-PDA nanoparticles were the same in all experiments).

tration of MnO_2 nanosheets. As depicted in Figure 3C, the fluorescence intensity ratio (F_0/F) of F-PDA nanoparticles was exponential with the concentration of MnO_2 nanosheets and there was no linear relationship between the F_0/F of F-PDA nanoparticles and the concentration of MnO_2 nanosheets. As a result, DQE was not the main mechanism in the fluorescence quenching process.

In conclusion, as analyzed above, FRET was considered to be the main possible mechanism for fluorescence quenching of F-PDA nanoparticles by MnO_2 nanosheets in this system.

Feasibility of the F-PDA−MnO_2 Probe for ALP Detection. Evidently, the quenched fluorescence of F-PDA nanoparticles was recovered when AA was added into the F-PDA−MnO_2 solution (Figure 4A). Also, we could clearly see that MnO_2 nanosheets were decomposed upon addition of AA into the MnO_2 solution or F-PDA−MnO_2 system from the TEM images (Figure 1B,C,F,G) and HRTEM images (the insets of Figure 1F,G), as well as the microstructure and morphology of the released F-PDA nanoparticles had almost no change after the reaction. As presented in Figure 2D, an obvious change of the UV−vis absorption spectrum of MnO_2 or F-PDA−MnO_2 occurred upon addition of a sufficient amount of AA. The characteristic absorption peak of MnO_2 nanosheets at 380 nm disappeared completely. Particularly, the absorbance spectrum of F-PDA−MnO_2−AA system was extremely close to that of F-PDA alone or F-PDA−Mn^{2+} system. Besides, both Mn^{2+} and MnO_2−AA system exhibited similar UV−vis absorption spectra where no peaks appeared and Mn^{2+} had almost no effect on the absorbance and fluorescence spectra (Figure 4A) of F-PDA nanoparticles. These phenomena directly corroborated that AA could trigger the reduction of MnO_2 nanosheets into Mn^{2+}. F-PDA nanoparticles were released, and meanwhile the fluorescence was recovered. Moreover, as shown in Figure 4B, the quenched fluorescence of F-PDA nanoparticles increased gradually when mixed with increasing concentration of AA and there was a good linear relationship from 1 to 100 μM (R^2 = 0.999), indicating that the sensing system could be well applied for further ALP detection.

The sensing mechanism for the detection of ALP is demonstrated in Figure 4C. The synthesized F-PDA nanoparticles exhibited an obvious high fluorescent signal (curve a in Figure 4C), and the mixture of F-PDA and AA2P (curve b in Figure 4C) almost presented the same signal with sole F-PDA nanoparticles after incubating for 40 min. Besides, when ALP was, respectively, added to the sole F-PDA nanoparticle solution and the mixed solution of F-PDA and AA2P, the fluorescence intensities remained almost unchanged under the same conditions (curves c and d in Figure 4C), indicating that AA2P and ALP had little effect on the fluorescence spectrum of F-PDA nanoparticles. The fluorescence of F-PDA nanoparticles was effectively quenched upon addition of MnO_2 nanosheets (curve e in Figure 4C), and the fluorescence signals showed almost no change when AA2P and ALP were, respectively, added into the F-PDA−MnO_2 solution after incubating for 40 min (curves f and g in Figure 4C). As ALP was added into the F-PDA−MnO_2−AA2P solution, the quenched fluorescence of F-PDA nanoparticles was obviously recovered owing to the destruction of MnO_2 nanosheets (curve h in Figure 4C). All of the above phenomena proved the F-PDA−MnO_2 fluorescent probe could be applied to detect ALP.

Optimization of Experimental Conditions. The F-PDA−MnO_2 fluorescent probe was sensitive to the coexistence of ALP and AA2P owing to the fact that MnO_2 nanosheets could be reduced by AA that was the hydrolysate of AA2P. Before investigating the effects on the fluorescence recovery of the sensing system, several experimental conditions were systematically performed to optimize the sensing conditions, including the concentrations of MnO_2 nanosheets and AA2P, as well as the effects of reaction time.

Obviously, the MnO_2 nanosheets concentration had a significant impact on the fluorescence intensity of F-PDA nanoparticles. As shown in Figure 3C, on the basis of the FRET mechanism, the fluorescence change at 458 nm of F-PDA nanoparticles exhibited an exponential decay with increased concentrations of MnO_2 nanosheets and the quenching efficiency increased with the increasing of MnO_2 nanosheet concentrations (Figure S4A). When the MnO_2 nanosheet concentration increased to 49.14 μg/mL, the quenching efficiency increased slowly and then achieved equilibrium and the quenching efficiency was up to 95% when the MnO_2 nanosheet concentration was 77.14 μg/mL. Considering that a lower concentration of MnO_2 nanosheets could not suppress the fluorescence of F-PDA nanoparticles fully and thus caused an inapparent fluorescence restoration change, on the contrary, a higher concentration of MnO_2 nanosheets could completely quench the fluorescence of F-PDA nanoparticles, causing AA to preferentially react with free MnO_2 nanosheets in solution in

DOI: 10.1021/acsami.7b18816
ACS Appl. Mater. Interfaces 2018, 10, 6560−6569

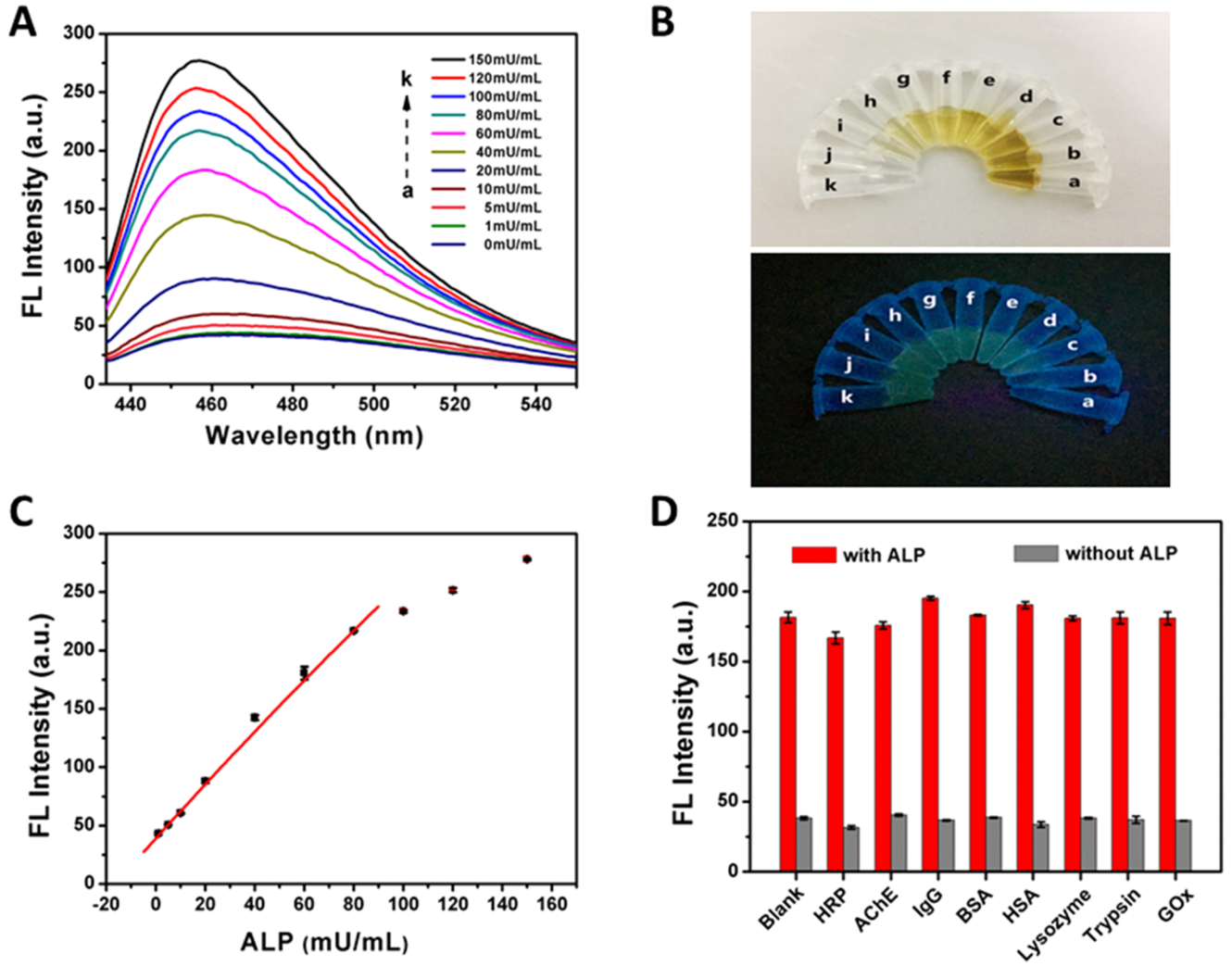

Figure 5. (A) Fluorescence emission spectra of the sensing system to different ALP concentrations. (from a to k : 0, 1, 5, 10, 20, 40, 60, 80, 100, 120, and 150 mU/mL). (B) The photographs showed the visual color change (top) and fluorescent color change (bottom) under 365 nm light of the sensing system corresponding to (A). (C) Fluorescence intensities at 458 nm versus different ALP concentrations. (D) Fluorescence responses of the biosensor against the control enzymes/proteins (20 μg/mL) in the absence and presence of ALP (60 mU/mL).

place of MnO_2 nanosheets combined with F-PDA nanoparticles, which resulted in poor sensitivity. Because of the two factors, we selected 49.14 μg/mL as the optimal concentration of MnO_2 nanosheets for the further assay.

In addition, the reaction times of the fluorescence quenching procedure and restoration procedure were also investigated. As the MnO_2 nanosheets were added into the F-PDA nanoparticle solution, the fluorescence quenching procedure was quite rapid and quickly reached a stable stage (Figure S4B), indicating that the F-PDA−MnO_2 nanocomposites were formed rapidly and easily. Hence, we chose 2 min as the reaction time of the fluorescence quenching procedure. As depicted in Figure S5, As ALP was added to F-PDA−MnO_2−AA2P solution, the fluorescence intensity progressively increased along with the increasing of enzymatic reaction time and then reached a balance after 40 min. Thus, 40 min was selected as the best time point for the subsequent experiments.

At last, we investigated the optimal concentration of AA2P and the results were shown in Figure S6. The fluorescence intensity at 458 nm of the sensing system increased gradually with the increasing of AA2P concentration and then reached the maximum value when the AA2P concentration was 3 mM in solution. As a result, we chose 3 mM as the optimal substrate concentration in the following experiments.

Quantitative Detection of ALP. Under the above optimal conditions, the linearity and detection limit of this sensing system were investigated. As presented in Figure 5A, the fluorescence intensity of F-PDA nanoparticles was gradually restored along with the increasing of ALP concentration and the fluorescence signal was almost restored completely when the ALP concentration increased to 150 mU/mL. In addition, the color of the solution was obviously observed to change from brown to colorless under natural light and 5 mU/mL of ALP activity could be easily found out by the naked eye. Meanwhile, the fluorescent color change of the solution also allowed a naked-eye readout under the ultraviolet lamp; similarly, 5 mU/mL of ALP activity could be detected and quasi-quantitatively identified (Figure 5B). Moreover, as exhibited in Figure 5C, we noticed that the restored fluorescence was closely related with ALP concentration and there was a good linear relationship between fluorescence intensities and ALP concentrations ranging from 1 to 80 mU/mL. The linear regression equation is $I = 39.60 + 2.22\ C_{[ALP]}$ (mU/mL), $R^2 = 0.999$. The detection limit of about 0.34 mU/

DOI: 10.1021/acsami.7b18816
ACS Appl. Mater. Interfaces 2018, 10, 6560−6569

Table 1. Recovery Analysis of ALP in Human Serum Samples

sample no.	1	2	3	4
amount of ALP added (mU/mL)	20	30	50	70
amount of ALP detected (mU/mL)	23.58 ± 0.95	34.84 ± 0.74	54.91 ± 2.12	75.03 ± 0.77
RSD (%)	2.29	1.41	2.92	0.83
recovery (%)	117.9 ± 4.7	116.1 ± 2.4	109.82 ± 4.2	107.2 ± 1.1

mL was obtained according to the calculation of three times the standard deviation, which was equal to or better than the previous reports for ALP determination (Table S2).

Specificity of the Sensing System. To further investigate the specificity of our sensing system toward ALP, the selectivity experiments of the biosensor were conducted via comparing the fluorescence intensity of the blank with that of the control enzymes/proteins, such as HRP, AChE, human IgG, BSA, HSA, lysozyme, trypsin, and GOx in the absence and presence of ALP (60 mU/mL). The results are shown in Figure 5D; obviously, the biosensor showed much higher fluorescence signal in the presence of only ALP and other nonspecific enzymes/proteins had no obvious interference on the fluorescence recovery of the sensing system. These results demonstrated that the proposed turn-on fluorescent biosensor exhibited excellent specificity and selectivity for ALP detection.

ALP Activity Assay in a Real Human Serum Sample. To evaluate the applicability of our proposed biosensor, the assay for ALP detection in real human serum samples was performed. The designed F-PDA−MnO_2 probe was applied to determine the recoveries by spiking a series of known concentrations of ALP in diluted human serum samples (5%). It is noteworthy that the interference from glutathione and cysteine in real samples can be eliminated via the addition of 0.3 mM NEM, a scavenger that can specifically react with glutathione and cysteine.[49] As presented in Table 1, the obtained recoveries ranged from 107.2 to 117.9%, with relative standard deviations (RSDs) ranging from 0.83 to 2.92%. These results have demonstrated that the proposed biosensor for ALP detection could be employed in the analysis of biological samples.

CONCLUSIONS

In summary, the reversible quenching effect of MnO_2 nanosheets on the fluorescence of F-PDA nanoparticles was found for the first time and we also intensively confirmed the quenching mechanism of FRET by using TEM, UV−vis, FT-IR spectroscopy, and fluorescence lifetime experiments. Inspired by such a quenching phenomenon, we further developed a "turn-on" sensing assay of ALP activity on the basis of the reduction of MnO_2 nanosheets to Mn^{2+} by AA, which is the enzymatic hydrolysate of ALP with AA2P as the substrate. The proposed biosensor presented following evident merits. First, the fluorescence nanomaterials used in this system were not only easily prepared, which could be carried out at room temperature and only for 90 min in the whole process, but also possessed good water solubility and photostability as well as excellent biocompatibility and biodegradability and then low concentration of MnO_2 nanosheets could reach high quenching efficiency and caused an exponential decay in fluorescence intensity of F-PDA nanoparticles. Last, the F-PDA−MnO_2 fluorescent probe strikingly achieved label-free, visual, cost-effective, and ultrasensitive detection of ALP, with the detection limit as low as 0.34 mU/mL, and it also presented excellent applicability in human serum samples. We believed that such a novel fluorescent probe would be potentially applied in bioimaging and other biological applications. Furthermore, our report may provide an avenue to expand the application of F-PDA nanoparticles to other nanomaterial-based biosensing systems.

ASSOCIATED CONTENT

Supporting Information

The Supporting Information is available free of charge on the ACS Publications website at DOI: 10.1021/acsami.7b18816.

FT-IR spectra of F-PDA−MnO_2 probe; fluorescence stability of F-PDA nanoparticles; the fluorescence intensity of F-PDA nanoparticles under different pH values; the fluorescence quenching efficiency and quenching time of F-PDA nanoparticles by MnO_2 nanosheets; optimization of enzymatic reaction time and AA2P concentration; the explanations about the interaction between F-PDA nanoparticles and MnO_2 nanosheets; the calculations corresponding to the quenching mechanism; and comparative table of performance of various immunoassays for ALP detection (PDF)

AUTHOR INFORMATION

Corresponding Author

*E-mail: xryang@ciac.ac.cn. Tel.: +86 431 85262056. Fax: +86 431 85689278.

ORCID

Jian Sun: 0000-0001-8964-6227

Xiurong Yang: 0000-0003-0021-5135

Author Contributions

The experiments and manuscript were mainly accomplished by T.X. under help and guidance of Prof. X.Y. and Dr. J.S. All authors have a contribution to the revision of the final manuscript.

Notes

The authors declare no competing financial interest.

ACKNOWLEDGMENTS

This work was supported by the National Key Research and Development Program of China (2016YFA0201301), the National Natural Science Foundation of China (Grant Nos. 21435005, 21627808, and 21605139), and Key Research Program of Frontier Sciences, CAS (QYZDY-SSW-SLH019).

REFERENCES

(1) Zheng, Z.; Chen, P.; Xie, M.; Wu, C.; Luo, Y.; Wang, W.; Jiang, J.; Liang, G. Cell Environment-Differentiated Self-Assembly of Nanofibers. *J. Am. Chem. Soc.* **2016**, *138*, 11128−11131.

(2) Zheng, F.; Guo, S.; Zeng, F.; Li, J.; Wu, S. Ratiometric Fluorescent Probe for Alkaline Phosphatase Based on Betaine-Modified Polyethylenimine via Excimer/Monomer Conversion. *Anal. Chem.* **2014**, *86*, 9873−9879.

DOI: 10.1021/acsami.7b18816
ACS Appl. Mater. Interfaces 2018, 10, 6560−6569

(3) Lin, L.; Liu, Y.; Yan, J.; Wang, X.; Li, J. Sensitive Nanochannel Biosensor for T4 Polynucleotide Kinase Activity and Inhibition Detection. *Anal. Chem.* **2013**, *85*, 334−340.
(4) Wang, Z.; Sun, N.; He, Y.; Liu, Y.; Li, J. DNA Assembled Gold Nanoparticles Polymeric Network Blocks Modular Highly Sensitive Electrochemical Biosensors for Protein Kinase Activity Analysis and Inhibition. *Anal. Chem.* **2014**, *86*, 6153−6159.
(5) Wolf, P. L. Clinical Significance of Serum High-molecular-mass Alkaline Phosphatase, Alkaline Phosphatase−lipoprotein-X Complex, and Intestinal Variant Alkaline Phosphatase. *J. Clin. Lab. Anal.* **1994**, *8*, 172−176.
(6) Fernandez, N. J.; Kidney, B. A. Alkaline Phosphatase: Beyond the Liver. *Vet. Clin. Pathol.* **2007**, *36*, 223−233.
(7) Dong, L.; Qian, J.; Hai, Z.; Xu, J.; Du, W.; Zhong, K.; Liang, G. Alkaline Phosphatase-Instructed Self-Assembly of Gadolinium Nanofibers for Enhanced T_2-Weighted Magnetic Resonance Imaging of Tumor. *Anal. Chem.* **2017**, *89*, 6922−6925.
(8) Kawaguchi, M.; Hanaoka, K.; Komatsu, T.; Terai, T.; Nagano, T. Development of a Highly Selective Fluorescence Probe for Alkaline Phosphatase. *Bioorg. Med. Chem. Lett.* **2011**, *21*, 5088−5091.
(9) Wei, H.; Chen, C.; Han, B.; Wang, E. Enzyme Colorimetric Assay Using Unmodified Silver Nanoparticles. *Anal. Chem.* **2008**, *80*, 7051−7055.
(10) Choi, Y.; Ho, N.-H.; Tung, C.-H. Sensing Phosphatase Activity by Using Gold Nanoparticles. *Angew. Chem., Int. Ed.* **2007**, *46*, 707−709.
(11) Li, G.; Fu, H.; Chen, X.; Gong, P.; Chen, G.; Xia, L.; Wang, H.; You, J.; Wu, Y. Facile and Sensitive Fluorescence Sensing of Alkaline Phosphatase Activity with Photoluminescent Carbon Dots Based on Inner Filter Effect. *Anal. Chem.* **2016**, *88*, 2720−2726.
(12) Freeman, R.; Finder, T.; Gill, R.; Willner, I. Probing Protein Kinase (CK2) and Alkaline Phosphatase with CdSe/ZnS Quantum Dots. *Nano Lett.* **2010**, *10*, 2192−2196.
(13) Goggins, S.; Naz, C.; Marsh, B. J.; Frost, C. G. Ratiometric Electrochemical Detection of Alkaline Phosphatase. *Chem. Commun.* **2015**, *51*, 561−564.
(14) Ino, K.; Kanno, Y.; Arai, T.; Inoue, K. Y.; Takahashi, Y.; Shiku, H.; Matsue, T. Novel Electrochemical Methodology for Activity Estimation of Alkaline Phosphatase Based on Solubility Difference. *Anal. Chem.* **2012**, *84*, 7593−7598.
(15) Jiang, H.; Wang, X. Alkaline Phosphatase-Responsive Anodic Electrochemiluminescence of CdSe Nanoparticles. *Anal. Chem.* **2012**, *84*, 6986−6993.
(16) Ruan, C.; Wang, W.; Gu, B. Detection of Alkaline Phosphatase Using Surface-Enhanced Raman Spectroscopy. *Anal. Chem.* **2006**, *78*, 3379−3384.
(17) Ingram, A.; Moore, B. D.; Graham, D. Simultaneous Detection of Alkaline Phosphatase and β-galactosidase Activity Using SERRS. *Bioorg. Med. Chem. Lett.* **2009**, *19*, 1569−1571.
(18) Hasegawa, T.; Masaru, S.; Kohei, T.; Hirotaka, M.; Tomonari, U.; Hiroki, H. Assay of Alkaline Phosphatase in Salmon Egg Cell Cytoplasm with Fluorescence Detection of Enzymatic Activity and Zinc Detection by ICP-MS in Relation to Metallomics Research. *Bull. Chem. Soc. Jpn.* **2006**, *79*, 1211−1214.
(19) Chen, J.; Jiao, H.; Li, W.; Liao, D.; Zhou, H.; Yu, C. Real-Time Fluorescence Turn-On Detection of Alkaline Phosphatase Activity with a Novel Perylene Probe. *Chem. - Asian J.* **2013**, *8*, 276−281.
(20) Gong, H.; Little, G.; Cradduck, M.; Draney, D. R.; Padhye, N.; Olive, D. M. Alkaline Phosphatase Assay Using a Near-infrared Fluorescent Substrate Merocyanine 700 Phosphate. *Talanta* **2011**, *84*, 941−946.
(21) Liu, S.; Wang, X.; Pang, S.; Na, W.; Yan, X.; Su, X. Fluorescence Detection of Adenosine-5′-triphosphate and Alkaline Phosphatase Based on the Generation of CdS Quantum Dots. *Anal. Chim. Acta* **2014**, *827*, 103−110.
(22) Liu, J.; Tang, D.; Chen, Z.; Yan, X.; Zhong, Z.; Kang, L.; Yao, J. Chemical Redox Modulated Fluorescence of Nitrogen-doped Graphene Quantum Dots for Probing the Activity of Alkaline Phosphatase. *Biosens. Bioelectron.* **2017**, *94*, 271−277.
(23) Qian, Z.; Chai, L.; Tang, C.; Huang, Y.; Chen, J.; Feng, H. Carbon Quantum Dots-Based Recyclable Real-Time Fluorescence Assay for Alkaline Phosphatase with Adenosine Triphosphate as Substrate. *Anal. Chem.* **2015**, *87*, 2966−2973.
(24) Hu, X. L.; Wu, X. M.; Fang, X.; Li, Z. J.; Wang, G. L. Switchable Fluorescence of Gold Nanoclusters for Probing the Activity of Alkaline Phosphatase and its Application in Immunoassay. *Biosens. Bioelectron.* **2016**, *77*, 666−672.
(25) Liu, H.; Li, M.; Xia, Y.; Ren, X. A Turn-On Fluorescent Sensor for Selective and Sensitive Detection of Alkaline Phosphatase Activity with Gold Nanoclusters Based on Inner Filter Effect. *ACS Appl. Mater. Interfaces* **2017**, *9*, 120−126.
(26) Li, Q.; Wang, C.; Tan, H.; Tang, G.; Gao, J.; Chen, C.-H. A Turn on Fluorescent Sensor Based on Lanthanide Coordination Polymer Nanoparticles for the Detection of Mercury(ii) in Biological Fluids. *RSC Adv.* **2016**, *6*, 17811−17817.
(27) Deng, J.; Yu, P.; Wang, Y.; Mao, L. Real-time Ratiometric Fluorescent Assay for Alkaline Phosphatase Activity with Stimulus Responsive Infinite Coordination Polymer Nanoparticles. *Anal. Chem.* **2015**, *87*, 3080−3086.
(28) Childress, E. S.; Roberts, C. A.; Sherwood, D. Y.; LeGuyader, C. L. M.; Harbron, E. J. Ratiometric Fluorescence Detection of Mercury Ions in Water by Conjugated Polymer Nanoparticles. *Anal. Chem.* **2012**, *84*, 1235−1239.
(29) Lin, Z.; Li, M.; Lv, S.; Zhang, K.; Lu, M.; Tang, D. In Situ Synthesis of Fluorescent Polydopamine Nanoparticles Coupled with Enzyme-controlled Dissolution of MnO_2 Nanoflakes for a Sensitive Immunoassay of Cancer Biomarkers. *J. Mater. Chem. B* **2017**, *5*, 8506−8513.
(30) Yildirim, A.; Bayindir, M. Turn-on Fluorescent Dopamine Sensing Based on in Situ Formation of Visible Light Emitting Polydopamine Nanoparticles. *Anal. Chem.* **2014**, *86*, 5508−5512.
(31) An, T.; Lee, N.; Cho, H.-J.; Kim, S.; Shin, D.-S.; Lee, S.-M. Ultra-selective Detection of Fe^{2+} Ion by Redox Mechanism Based on Fluorescent Polymerized Dopamine Derivatives. *RSC Adv.* **2017**, *7*, 30582−30587.
(32) Zhang, A.; Neumeyer, J. L.; Baldessarini, R. J. Recent Progress in Development of Dopamine Receptor Subtype-Selective Agents: Potential Therapeutics for Neurological and Psychiatric Disorders. *Chem. Rev.* **2007**, *107*, 274−302.
(33) Liu, Y.; Ai, K.; Lu, L. Polydopamine and Its Derivative Materials: Synthesis and Promising Applications in Energy, Environmental, and Biomedical Fields. *Chem. Rev.* **2014**, *114*, 5057−5115.
(34) Kong, J.; Yee, W. A.; Wei, Y.; Yang, L.; Ang, J. M.; Phua, S. L.; Wong, S. Y.; Zhou, R.; Dong, Y.; Li, X.; Lu, X. Silicon Nanoparticles Encapsulated in Hollow Graphitized Carbon Nanofibers for Lithium Ion Battery Anodes. *Nanoscale* **2013**, *5*, 2967−2973.
(35) Yang, S. H.; Kang, S. M.; Lee, K.-B.; Chung, T. D.; Lee, H.; Choi, I. S. Mussel-Inspired Encapsulation and Functionalization of Individual Yeast Cells. *J. Am. Chem. Soc.* **2011**, *133*, 2795−2797.
(36) Zhang, P.-H.; Cao, J.-T.; Min, Q.-H.; Zhu, J.-J. Multi-Shell Structured Fluorescent−Magnetic Nanoprobe for Target Cell Imaging and On-Chip Sorting. *ACS Appl. Mater. Interfaces* **2013**, *5*, 7417−7424.
(37) Gao, H.; Sun, Y.; Zhou, J.; Xu, R.; Duan, H. Mussel-Inspired Synthesis of Polydopamine-Functionalized Graphene Hydrogel as Reusable Adsorbents for Water Purification. *ACS Appl. Mater. Interfaces* **2013**, *5*, 425−432.
(38) Bally, M.; Vörös, J. Nanoscale Labels: Nanoparticles and Liposomes in the Development of High-performance Biosensors. *Nanomedicine* **2009**, *4*, 447−467.
(39) Kong, X.-J.; Wu, S.; Chen, T.-T.; Yu, R.-Q.; Chu, X. MnO_2-induced Synthesis of Fluorescent Polydopamine Nanoparticles for Reduced Glutathione Sensing in Human Whole Blood. *Nanoscale* **2016**, *8*, 15604−15610.
(40) Zhao, Y.-Y.; Li, L.; Yu, R.-Q.; Chen, T.-T.; Chu, X. CoOOH-induced Synthesis of Fluorescent Polydopamine Nanoparticles for the Detection of Ascorbic Acid. *Anal. Methods* **2017**, *9*, 5518−5524.
(41) Lin, J.-H.; Yu, C.-J.; Yang, Y.-C.; Tseng, W.-L. Formation of Fluorescent Polydopamine Dots from Hydroxyl Radical-induced

DOI: 10.1021/acsami.7b18816
ACS Appl. Mater. Interfaces 2018, 10, 6560−6569

Degradation of Polydopamine Nanoparticles. *Phys. Chem. Chem. Phys.* **2015**, *17*, 15124−15130.
(42) Fan, D.; Shang, C.; Gu, W.; Wang, E.; Dong, S. Introducing Ratiometric Fluorescence to MnO_2 Nanosheet-Based Biosensing: A Simple, Label-Free Ratiometric Fluorescent Sensor Programmed by Cascade Logic Circuit for Ultrasensitive GSH Detection. *ACS Appl. Mater. Interfaces* **2017**, *9*, 25870−25877.
(43) Kai, K.; Yoshida, Y.; Kageyama, H.; Saito, G.; Ishigaki, T.; Furukawa, Y.; Kawamata, J. Room-Temperature Synthesis of Manganese Oxide Monosheets. *J. Am. Chem. Soc.* **2008**, *130*, 15938−15943.
(44) Deng, R.; Xie, X.; Vendrell, M.; Chang, Y.-T.; Liu, X. Intracellular Glutathione Detection Using MnO_2-Nanosheet-Modified Upconversion Nanoparticles. *J. Am. Chem. Soc.* **2011**, *133*, 20168−20171.
(45) Zhijiang, C.; Chengwei, H. Study on the Electrochemical Properties of Zinc/Polyindole Secondary Battery. *J. Power Sources* **2011**, *196*, 10731−10736.
(46) Zhai, W.; Wang, C.; Yu, P.; Wang, Y.; Mao, L. Single-Layer MnO_2 Nanosheets Suppressed Fluorescence of 7-Hydroxycoumarin: Mechanistic Study and Application for Sensitive Sensing of Ascorbic Acid in Vivo. *Anal. Chem.* **2014**, *86*, 12206−12213.
(47) Wang, Y.; Jiang, K.; Zhu, J.; Zhang, L.; Lin, H. A FRET-based Carbon Dot-MnO_2 Nanosheet Architecture for Glutathione Sensing in Human Whole Blood Samples. *Chem. Commun.* **2015**, *51*, 12748−12751.
(48) Lin, L.; Liu, Y.; Zhao, X.; Li, J. Sensitive and Rapid Screening of T4 Polynucleotide Kinase Activity and Inhibition Based on Coupled Exonuclease Reaction and Graphene Oxide Platform. *Anal. Chem.* **2011**, *83*, 8396−8402.
(49) Yuan, J.; Cen, Y.; Kong, X.-J.; Wu, S.; Liu, C.-L.; Yu, R.-Q.; Chu, X. MnO_2-Nanosheet-Modified Upconversion Nanosystem for Sensitive Turn-On Fluorescence Detection of H_2O_2 and Glucose in Blood. *ACS Appl. Mater. Interfaces* **2015**, *7*, 10548−10555.

DOI: 10.1021/acsami.7b18816
ACS Appl. Mater. Interfaces 2018, 10, 6560−6569